Effect of Gauge Length on Distributed Acoustic Sensing Performance for Baleen Whale Monitoring

Marie-Ève Clark*,
Email: marie-eve.clark@uqar.ca
Pierre Cauchy*, Stéphane Blouin†, and Léa Bouffaut‡,
*Institut des sciences de la mer, Université du Québec à Rimouski, Rimouski, QC, Canada
†Département de génie électrique, École de technologie supérieure (ÉTS), Montréal, QC, Canada
‡Cornell K. Lisa Yang Center for Conservation Bioacoustics, Cornell University, Ithaca, NY, USA

***Abstract*—Distributed Acoustic Sensing (DAS) converts underwater fiber-optic cables into dense sensor arrays for marine monitoring, including ship and baleen whale detection. Detection performance is governed by the gauge length (GL), an acquisition setting set as a trade-off between optical signal-to-noise ratio (SNR) and bandwidth. Longer GLs improve optical SNR by integrating more backscattered light into strain measurements, at the cost of reduced frequency response.**

Here, we investigate the effect of the GL on strain amplitude, SNR, and noise floors using data collected on a telecommunication cable crossing the St. Lawrence Estuary in Quebec, Canada with a FOSINA DxS interrogator during controlled-source playbacks. Raw optical data were processed with GLs of 5 to 20 m. Analysis of a playback tone at 100 Hz shows that increasing the GL reduced measured noise levels, with a GL of 10 m providing the best SNR overall, generally consistent with theoretical predictions. The estimated pressure-to-strain conversion factor increased systematically with GL by 0.76-0.77 dB/m, indicating a potential GL dependence not fully captured by the theoretical DAS response model considered here. The findings of this work provide an empirical basis for GL selection for monitoring whale calls near 100 Hz, while demonstrating that optimal configuration remains considerably influenced by the source-to-cable geometry.

***Index Terms*—Distributed Acoustic Sensing, telecommunication cables, marine mammal monitoring, fiber optic, underwater monitoring, acoustic detection, acoustic playbacks**

I. Introduction

Distributed Acoustic Sensing (DAS) transforms fiber-optic cables into dense arrays of strain sensors [1]. Underwater acoustic waves generate pressure fluctuations, producing small dynamic strain along the cable and enabling observations of vessels [2]–[4] and baleen whales [4]–[7] localized over large areas. DAS data can also be accessed in real time. Expanding human use of the ocean increases the risk of harmful interactions between anthropogenic activities and marine life [8]. Therefore, there is a growing need for monitoring systems that provide broad spatial coverage, real-time data access, and scalable monitoring [9], [10]. Given these characteristics and the geographical extent of existing submarine cable networks, DAS represents a promising tool for marine monitoring that could support both long-term ecological observations and time-sensitive conservation measures.

Most marine mammal studies using DAS on existing submarine telecommunication cables have focused on low-frequency baleen whale vocalizations, particularly of blue and fin whales, between $10-80$ Hz [5]–[7]. Yet, baleen whale species produce vocalizations with energy at higher frequencies, many within the 100–200 Hz range, such as the bowhead (*Balaena mysticetus*), humpback (*Megaptera novaeangliae*), sei (*Balaenoptera borealis*) and the critically endangered North Atlantic right whales (*Eubalaena glacialis*) [11]–[14]. For DAS to serve as an effective monitoring tool, its performance and limitations must first be quantified, as is done for other passive acoustic monitoring (PAM) systems. Ecological measurements such as occurrence, occupancy, abundance, as well as real-time monitoring for timely mitigation, require characterization of technological performance to ensure that observations can be interpreted appropriately [15]. For DAS, this includes investigating its frequency response and sensitivity across marine mammal-relevant bandwidths, the influence of system noise on detection range, and the effects of fiber and cable configuration on detection and localization performance [16]. These characteristics are needed to define the effective surveyed area and quantify detection probability for ecological monitoring applications.

The gauge length (GL) is one of the most important DAS acquisition parameters. It corresponds to the section of fiber over which DAS measures strain by differentiating the phase of the backscattered light [1], [17]. The GL acts as a moving spatial averaging window and represents a tradeoff between optical signal-to-noise ratio (SNR) and bandwidth. A longer GL integrates more backscattered light, improving optical SNR, but it also reduces the measured signal amplitude as the signal wavelength approaches or becomes shorter than the GL. Furthermore, the response becomes increasingly directional at

DAS data collection and playbacks in Canada were supported by the Natural Sciences and Engineering Research Council of Canada (NSERC) under Alliance Grant (ALLRP 598039-24), Centre for Ocean Ventures & Entrepreneurship (COVE) under Research Agreement #2026-003 and WWF Canada through Grant Agreement #G-1025-1149-00-D. MEC was additionally supported through Canada Graduate Scholarships–Master's program (CGS M) and the Fonds de recherche du Québec (FRQ) Master's Research Scholarship.

higher frequencies for longer GLs [18].

The SNR-optimizing GL is theoretically defined as approximately 0.58λ, where λ is the apparent spatial wavelength of the signal of interest [17]. For the simple axial case, where propagation is parallel to the cable, a 100 Hz signal propagating at the speed of sound in seawater (here 1460 m/s) gives an optimal GL $\sim$ 8.5 m, and slightly longer for signals propagating at higher speeds through soft sediments. A proposed revision based on a signal-preservation optimization criterion sets the optimizer to 0.47λ [19], which corresponds to a GL ~ 6.9 m for the same 100 Hz signal.

For marine mammal monitoring, the apparent wavelength depends on the bandwidth and the propagation direction of their vocalizations relative to the cable orientation. GLs ranging from a few meters to a few tens of meters are commonly chosen for marine DAS data collection [4], [6], but the influence of this choice on signal detectability has received limited *in situ* evaluation on telecommunication cables. A relevant step in performance assessment is to characterize DAS response to higher-frequency signals, where the effects of acquisition parameters become increasingly important [17]. Here, we use a controlled playback experiment and process raw data with multiple GLs from the same recorded signals to compare their effects under identical conditions. We quantify the DAS response with signal amplitude and SNR, and we compare it with theoretical levels to inform GL selection for the 100 Hz frequency.

II. Methods

A. Data collection

1) Raw Optical DAS data: In August 2025, we collected DAS data on a telecommunication cable owned by TELUS located between Forestville and Le Bic, in the St. Lawrence Estuary (Quebec, Canada). We instrumented a fiber of this cable with a FOSINA DxS interrogator, installed at the cable landing station in Forestville[0]. During the playbacks, we collected raw optical phase data over a 30-km cable section, between 8 and 38 km. Raw optical phase data collection only requires defining the pulse width and pulse rate, here set to 5.10 m and $1,250$ Hz. Other acquisition settings (e.g., sample rate, channel spacing, gauge length) are chosen in post-processing, enabling the comparison of the same signal exported with different parameters. Note that the pulse width and pulse rate respectively constrain the minimum GL and maximum sample rate for data exports.

2) Cable position: Cable cumulative distance and deployment geometry were initially obtained from TELUS fiber-lay and fiber repair routes. Updated cable geometry and burial state (visible or not visible) were derived from side-scan sonar data acquired in June 2026 with a Klein 3000 system[1] and an Advanced Navigation geopositioning system during a dedicated survey. TELUS fiber-lay and sonar coordinates were aligned using distinctive bends in the cable as positional anchors. At locations where the cable was not visible in the sonar data, its geometry was reconstructed using the corresponding section of the original cable route and adjusted to connect adjacent visible sections. For spatial alignment of the DAS data, we determined the portion of cable laid on land by a shore-based tap test at the Forestville landing. The resulting offset was $2,940\pm10$ m. Fig. 1 is a positional map of the study area with reconstructed cable geometry and playback sites (PS) near a cable bend, at a depth of ~ 155 m.

3) Bathymetric data: Bathymetric data were obtained from the Canadian Hydrographic Service[2] and water depth from the average water level of neighboring tide stations[3]. Parameters were interpolated along the cable based on side-scan sonar cable coordinates and reconstructed geometry.

4) Active source: On August 21, 2025, we conducted controlled, georeferenced playbacks of synthetic signals at multiple cross-line distances from the fiber using an omnidirectional Lubell VC2C[4] underwater speaker, with a usable frequency range of 50–$1,500$ Hz and a resonant frequency of 115 Hz. Playback sites are abbreviated as PS, with respective offsets of PS01: 0 m, PS02: 100 m, PS03: 200 m, PS04: 400 m. Fig. 1 shows the average position across five repeated emissions at each PS. The playback protocol we followed (e.g., source signals, setup, metadata, etc.) is available for reproducibility [20]. A calibrated reference hydrophone (Reson TC4032[5]) was positioned 1 m above the source for source level estimation, sampling data at 12.8 kHz with 24-bit resolution. An acceleration data logger (Star-Oddi, Starmon tilt[6]) recorded an average speaker depth of 9.94 m.

5) DAS data selection and exports: This work addresses the 3 km cable section surrounding PS01 (Fig. 1). The raw optical DAS data corresponding to each PS were exported with a sampling frequency of 625 Hz, a 2.04 m channel spacing (interval between DAS channels) and at multiple GLs: 5.10, 6.12, 8.16, 10.20, 12.24, 20.42 m. The GL values are presets of the DxS post-processing software and are rounded for simplicity in the remainder of this document. The presented work focuses on the 100 Hz tonal signal (1 s-long) from the playback series. Playback timestamps and locations were used to extract and process the corresponding signal windows.

B. Theoretical overview

To investigate the influence of GL on the performance of DAS, we follow the DAS passive sonar equation framework [21] where the received level in strain ($RL_{\mathrm{dB\,re\,1\,\mu\varepsilon}}$) corresponds to

$$RL_{\mathrm{dB\,re\,1\,\mu\varepsilon}} = RL_{\mathrm{dB\,re\,1\,\mu Pa}} + S_{\mathrm{Pa}\to\varepsilon} + H_{\mathrm{DAS}_\varepsilon}, \qquad (1)$$

with $RL_{\mathrm{dB\,re\,1\,\mu Pa}}$ the received pressure level at the location of the fiber, $S_{\mathrm{Pa}\to\varepsilon}$ the pressure-to-strain conversion factor,

[0] https://fosina.fr/innovation/

[1] https://kordil.com/distributorships/kleinmarinesystems/klein-system-3000

[2] Bathymetric data from the Canadian Hydrographic Service accessible from https://data.chs-shc.ca/dashboard/map/

[3] Tide station data accessible from https://www.marees.gc.ca/en/stations

[4] https://www.lubell.com/products/vc2c/

[5] https://www.teledynemarine.com/brands/reson/tc-4032

[6] https://www.star-oddi.com/products/data-loggers/acceleration-tilt-logger

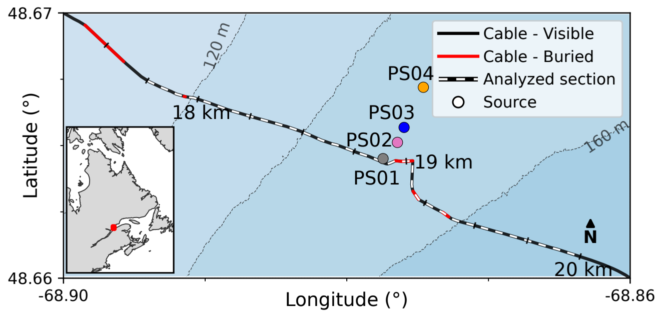

Fig. 1. Map of the 2025 St. Lawrence georeferenced playback experiment for *in situ* characterization of DAS performance. A FOSINA DxS interrogator was installed in Forestville on a cable crossing the St. Lawrence Estuary in Quebec, Canada (TELUS Sunoque II). This analysis focuses on the 17.75–20 km section where we conducted playbacks of synthetic signals, indicated as colored dots at multiple cross-line distances from the fiber by playback site (PS). The local geometry of the fiber creates multiple locations where the grazing angle $\theta \to 90°$(apex): PS01 at 18.88 and 19.04 km, PS02 at 18.90 and 18.95 km, PS03 at 18.90 and 19.00 km and PS04 at 18.90 km. Reconstructed buried cable sections are red.

and $H_{\text{DAS}_\varepsilon}$ the response of DAS, modeled after [22]. The methods used to determine each of these terms are described in the following sections.

C. Data processing

1) Measured $RL_{\text{dB re 1}\,\mu\varepsilon}$: Data were converted from optical phase to strain and filtered using the *DAS4Whales* python package [23]. Following [21], a hybrid filter combining frequency-wavenumber (f-k) (1450–5000 m/s with a taper of $\pm$100 m/s for gradual attenuation) and bandpass filtering (98-102 Hz) was applied. The filtered data were then time-aligned by compensating for acoustic propagation travel time using a fixed sound speed of 1460 m/s and cable geometry (see [21] Fig. 2).

$RL_{\text{dB re 1}\,\mu\varepsilon}$ was measured across all DAS channels in the analysis window, for each 100 Hz tone, by averaging the received signal root-mean-square (RMS) strain amplitude in a 1-s window and converting to $\text{dB re 1}\,\mu\varepsilon$. The associated RMS noise level (NL) two seconds prior to each signal repetition was similarly estimated. The SNR was calculated on each channel per repetition as $\text{SNR} = 20\log 10\,(RL/NL)$, with no background noise subtraction for RL.

Median values for the five repetitions at each PS were used to represent the GL effect on the received signals (Fig. 2 and Fig. 3(a)). For visualization of the GL effect on noise floor and $S_{\text{Pa}\to\varepsilon}$, the median values of each repetition were pooled across the four PSs. Statistical assessment of GL dependence was performed separately, as described in Section II-D.

2) $RL_{\text{dB re 1}\,\mu\text{Pa}}$ estimation: We estimated $RL_{\text{dB re 1}\,\mu\text{Pa}}$ as the difference between the source level (SL) and the transmission loss (TL).

a) SL estimation: SL for the 100 Hz tone was estimated from measurements made by the reference hydrophone. We averaged the linearized RMS acoustic levels from 45 recorded repetitions (bandpass filter $98 - 102$ Hz; 1-s time window), resulting in $SL = 165 \pm 0.2$ dB re 1 μPa. We then used two approaches to estimate TL: propagation modeling and geometrical spreading with the Lloyd's mirror effect.

b) TL estimation: For the modeling approach, TL was first computed using the parabolic equation propagation model RAMGeo [24] based on Collins' split-step Padé solution [25]. Propagation was modeled for frequencies between 0.5-$1,500$ Hz, with a step of 0.5 Hz. We used a fixed sound speed of 1480 m/s based on a nearby 330 m CTD cast. The mean sound speed near the shallower cable section analyzed here was later found to be 1460 m/s. Subsequent modeling showed that this difference had a negligible effect on RL for cable sections more than 40 m from the source. Modeling parameters are given in Table I.

TABLE I
PARAMETERS USED FOR ACOUSTIC PROPAGATION MODELING.

Parameter	Value	Unit	Reference
Frequency step (f)	0.5	Hz	-
Radial step (Δr)	$10, 1600/f$	m	-
Vertical step (Δz)	$0.3, 48/f$	m	-
Maximum depth ($z_{\max}$)	600	m	-
Reference sound speed (c)	1480	m/s	-
Number of Padé terms ($n_{\text{Padé}}$)	4, 8	–	-
Stability constraint (n_{stab})	1	–	-
Stability range (r_{stab})	0	m	-
Sound speed in sediments ($c_{p,\text{sed}}$)	1612.5	m/s	[26], [27]
Sediment density (ρ_{sed})	1.8	g/cm^3	[26], [27]
Sediment absorption ($\alpha_{p,\text{sed}}$)	0.9	dB/λ_{sed}	[26], [27]
Sediment thickness	45	m	[28]
Sound speed in bedrock ($c_{p,\text{bed}}$)	5207.5	m/s	[27], [29]
Bedrock density (ρ_{bed})	2.6	g/cm^3	[27], [29]
Bedrock absorption ($\alpha_{p,\text{bed}}$)	0.1	dB/λ_{bed}	[26]

Note: The bedrock sound speed and density correspond to the averages of the values reported for green sandstone and quartzite by [29]. Under 1 km, Δr is halved, and $n_{\text{Padé}}$=8.

The modeling originally used the position of the first repetition of each PS. To account for the vessel's drift (max 60 m), we recalculated TL for each repetition using its three-dimensional source-to-channel distance while retaining the channel-specific propagation loss coefficient from the first repetition.

As a comparison point to [21], we also estimated TL using geometrical spreading and the Lloyd's mirror effect, with a transition range (r_T) from spherical to cylindrical. The transition range (r_T) was empirically defined as 4.5 times the water depth at the apex, to match with the modeled TL.

3) $H_{\text{DAS}_\varepsilon}$ modeling: The DAS response introduced in Eq. (1) is theorized as the cumulative effects of the gauge length (G_{GL}) and the coupling response between the fiber and the cable (G_κ) [21], [22]. The former mainly depends on the signal's wavelength (c/f), the gauge length (GL), the pulse width (L_W) and the grazing angle (θ) such as

$$G_{GL} = \text{sinc}\left(\frac{\pi f}{c} GL \cos\theta\right) \text{sinc}\left(\frac{\pi f}{c} L_W \cos\theta\right), \qquad (2)$$

while the latter mainly varies with θ, which is obtained from the cable geometry and known source positions.

4) $S_{\text{Pa}\to\varepsilon}$ estimation: Estimating the pressure-to-strain conversion factor corresponds to finding the value that minimizes the absolute error between measured and simulated

$RL_{\mathrm{dB\,re\,1}\,\mu\varepsilon}$. For each PS and GL, this value was obtained as the median difference between the two RLs across channel–repetition observations. To avoid angle-dependent response nulls, reduce noise influence, and limit uncertainties related to cable geometry, the following criteria were used to select the channels used for estimating $S_{\mathrm{Pa}\to\varepsilon}$:

- Channels between 18.25 and 18.75 km with $30° \leq \theta \leq 50°$ were retained because they showed a strong signal response and the corresponding cable section was geolocated by side-scan sonar.
- Channels near $\theta_{\mathrm{null}} = \arccos[c/(f\,GL)]$ over 98–102 Hz were excluded using a 0.75° angular margin, as they produce nulls.

D. Statistics

For each PS and repetition, the percentage of channels with SNR > 3 dB was calculated for each GL and summarized as the mean $\pm$ standard deviation. The effect of GL was assessed using a one-way repeated measures ANOVA, followed by paired t-tests with Holm-adjusted p-values ($\alpha = 0.05$).

The dependence of $S_{\mathrm{Pa}\to\varepsilon}$ and NL on GL was assessed using data matched across the six GLs. For $S_{\mathrm{Pa}\to\varepsilon}$, median values across repetitions were determined for each channel and centered across GL to estimate the slope. Then, a median slope was calculated from the pooled channel-median values with equal weighting across PSs. The correlation was evaluated using R^2 and RMSE. For NL, linear and fixed theoretical logarithmic ($NL = C - 20\log_{10} GL$) models were fitted to repetition-level channel medians and compared using R^2 and RMSE. The fixed model represents the expected variation with GL of instrumental strain noise arising from GL-independent phase estimation error [17]. We estimated uncertainty for slopes using 2000 hierarchical bootstrap iterations that resampled GL-matched repetitions with spatial blocks of 25 channels with replacement. A GL-related trend was supported when the 95% bootstrap CI excluded zero.

Differences in $S_{\mathrm{Pa}\to\varepsilon}$ between the two TL methods were evaluated from paired estimates matched by PS, repetition, channel and GL. The median paired difference ($S_{\mathrm{Pa}\to\varepsilon,\mathrm{TLgeometrical}} - S_{\mathrm{Pa}\to\varepsilon,\mathrm{TLmodeling}}$) and its interquartile range (IQR) were reported. Uncertainty was estimated using the same hierarchical bootstrap procedure described above, with equal weighting across PSs for the pooled estimate. We considered the difference between $S_{\mathrm{Pa}\to\varepsilon}$ to be supported when the 95% bootstrap CI excluded zero.

III. Results

The influence of the gauge length on DAS signal and noise levels was first assessed across four playback sites. Fig. 2 shows the median SNR along the analyzed cable section. The statistical analysis indicated that, although differences between neighboring GLs were not always statistically significant, GL10 consistently ranked among the GLs with the highest proportion of channels exceeding the 3 dB SNR threshold. Although not as consistent across PSs, similar performances were observed for GL8 and GL12. Channels with high SNR were predominantly located within approximately 750 m of one of the cable apexes and were associated with grazing angles θ greater than 20°and $<$ 90°. GL20 produced the highest SNR at specific channels. However, this enhanced response was spatially localized and appeared primarily at $\theta > 30°$. Its overall performance also varied between PS and repetitions, ranking among the highest-performing statistical groups at PS01 and PS02, while overlapping with the lowest-performing group at PS02, PS03, and PS04. Across all PS-GL combinations, the mean number of channels with SNR > 3 dB ranged from 398 (36%) for GL5 (PS01) to 553 (52%) for GL10 (PS03).

Fig. 3(a) presents an example of the difference in RMS strain level for two GLs at PS03, along the cable. The difference in measured strain from the 100 Hz signal between GL6 and GL12 varies spatially, being generally smaller from 18.5 to the 18.9 km apex, and larger beyond it. The theoretical strain levels from both TL methods match the general shape of the measured strain where $RL > NL$, prior to the 18.9 km apex, and less so past it ($>$ 19.25 km), where the cable's geometry is more complex (Fig. 1).

For all PSs combined, the decrease in NL with increasing GLs (Fig. 3(b)) was best fitted with a linear model, with a rate of -0.70 dB/m ($R^2 = 0.99$, RMSE $= 0.27$ dB, 95% CI: -0.71 to -0.69 dB/m), in comparison to the fixed theoretical logarithmic model ($R^2 = 0.92$). Median NL showed a 10.3 dB difference between GL6 (-85.4 dB re 1 $\mu\varepsilon$) and GL20 (-95.7 dB re 1 $\mu\varepsilon$).

Across matched observations from all PSs and GLs, the median paired difference in $S_{\mathrm{Pa}\to\varepsilon}$ between the geometrical and modeled TL methods (Fig. 3(c)) was 4.15 dB (IQR: 3.25–4.95 dB; 95% bootstrap CI: 3.64–4.46 dB). The CI excluding zero supports a difference in $S_{\mathrm{Pa}\to\varepsilon}$ between the two theoretical RL models. Across PSs, both models show a very similar dependence on GL, with a 0.77 dB/m ($R^2 = 0.94$, RMSE $= 0.92$ dB, 95% CI: 0.64 to 1.01 dB/m) coefficient estimate for the geometrical propagation, and 0.76 dB/m ($R^2 = 0.94$, RMSE $= 0.91$ dB, 95% CI: 0.64 to 1.00 dB/m) for the modeled one.

IV. Discussion

This work examines how the gauge length influences the response of DAS to a 100 Hz tone, with a fixed pulse width, and compares the observations with theoretical predictions. Differences between the two transmission-loss approaches used to estimate acoustic pressure resulted in a 4 dB difference in the inferred $S_{\mathrm{Pa}\to\varepsilon}$, highlighting the importance of appropriate acoustic propagation modeling when estimating received strain levels. The match between the theoretical responses calculated from Eq. 1 and the measured received levels also varied along the cable. Although the analyzed cable section was mostly unburied and located at a relatively uniform depth, variations in cable-substrate coupling associated with small-scale seafloor morphology (e.g., local suspension over dunes or rocks) may have contributed to these discrepancies. Imperfect alignment between cumulative DAS channel distance and the

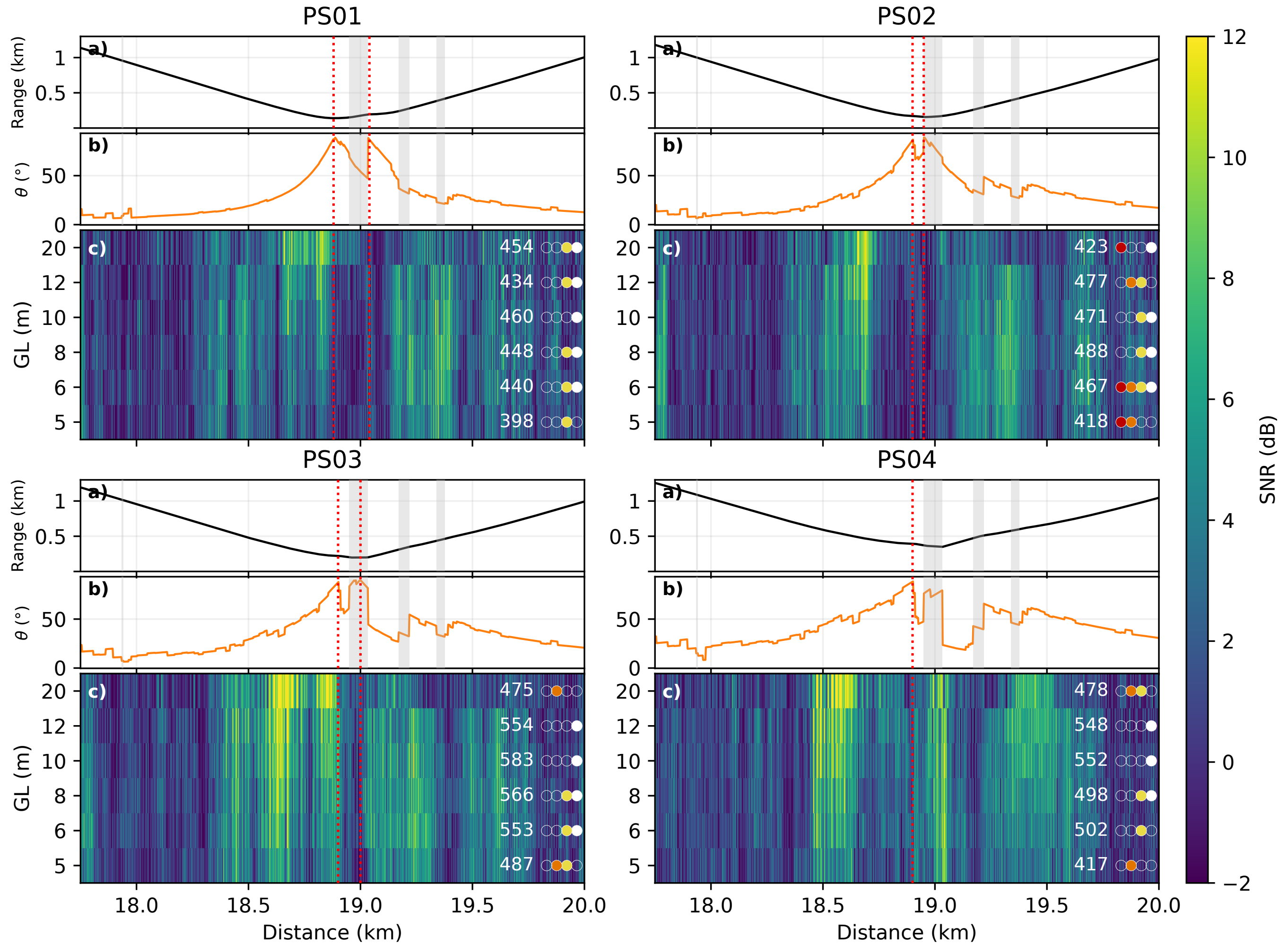

Fig. 2. Influence of the gauge length and cable geometry on insonified channels at four playback locations. Per playback site: (a) 3D distance between the source and the cable, (b) grazing angle (θ) averaged across repetitions, and (c) SNR by GL, represented over our defined cable section of interest between 17.75 and 20 km. Red dotted lines indicate the apex positions ($\theta = 89°$-$90°$) and grayed out areas in (a) and (b) indicate unknown cable geometry from buried cable sections. Colored dots on (c) identify statistically homogeneous groups. Within each PS, GLs that don't share dots have a significantly different percentage of channels with SNR > 3 dB according to Holm-corrected paired comparisons ($\alpha = 0.05$). White identifies the group with the highest percentage, and numbers show the median channel count above threshold.

sonar-surveyed cable sections may have introduced additional spatial mismatch between the theoretical and observed strain levels.

Variability in the pressure-to-strain conversion factor shown in Fig. 3(c) within a given GL primarily reflected differences in $S_{\mathrm{Pa}\to\varepsilon}$ between PSs. These differences could be due to PS-specific source-to-cable geometries associated with increasing source range. Despite PSs being pooled to reduce the influence of these geometrical effects, and despite restricting the analysis to the same cable section and grazing angle interval, $S_{\mathrm{Pa}\to\varepsilon}$ increased systematically with GL ($0.76 - 0.77$ dB/m). Together with the small RMSE (0.92 dB), this trend suggests that the formulation of $H_{\mathrm{DAS}_\varepsilon}$ based on G_{GL} and G_κ in Eq. 1, may not fully capture the effect of GL on the measured strain response. However, because the analysis required channels to be matched across all GLs, trend estimation was limited to 25–58 channels per PS. The observed relationship should therefore be interpreted with some caution. Nevertheless, the systematic increase contrasts with previously reported fixed conversion factors at lower frequencies, including -187.2 dB at 20 Hz [21] and -177.7 ± 3.5 dB at 30-50 Hz [30], obtained across different cables and GLs using the same geometrical TL equations applied here.

The observed decrease in NL with increasing GL is consistent with theoretical expectations [17], [19]. However, our measured trend of ~ -0.70 dB/m was better described by a linear model than by the theoretical dependence [17], suggesting that additional noise processes may have contributed to the observed trend. The fixed pulse width of 5.10 m may also have influenced our observations. A pulse width greater than ~ 0.56GL is expected to have a stronger effect on the response than the GL itself [31], corresponding to a transition

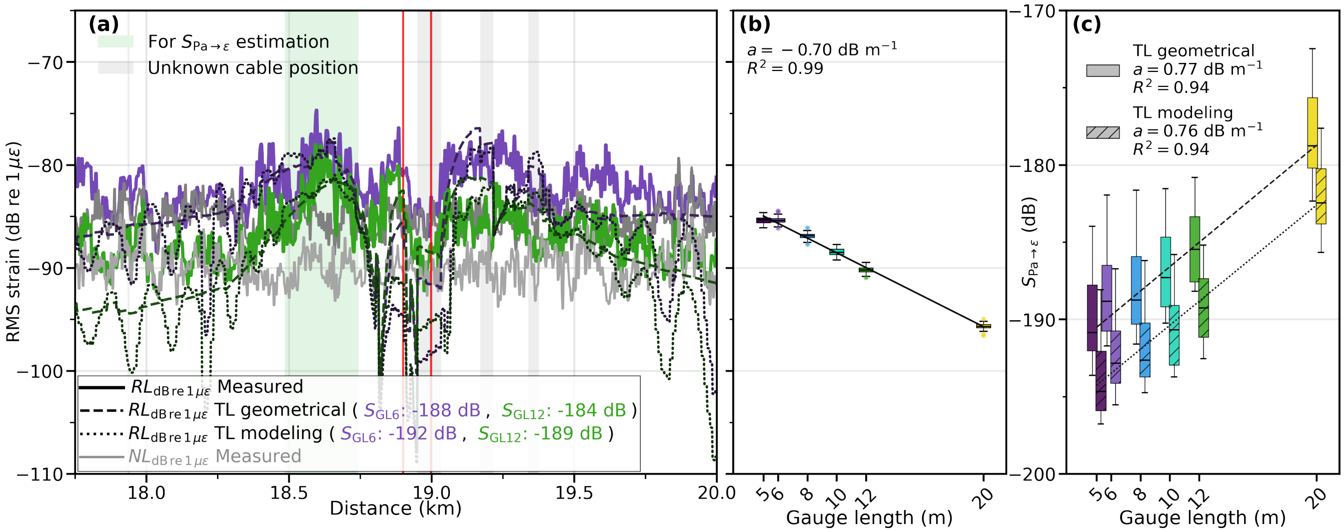

Fig. 3. Effect of the gauge length on received levels, noise floor and conversion factor between Pascal and strain ($S_{\mathrm{Pa}\rightarrow\varepsilon}$). (a) Median root-mean-square signal and noise at 100 Hz for PS03 with theoretical level curves from equation 1 for GL6 and GL12. Red lines indicate apexes ($\theta = 89 - 90°$). (b) Distribution of median RMS noise levels at 100 Hz across playback repetitions for pooled channels between 17.75 and 20 km, with all PSs combined ($n_{rep} = 20$). (c) Distribution of pressure-to-strain ($S_{\mathrm{Pa}\rightarrow\varepsilon}$) conversion factor from matched channels, estimated using geometrical and modeled transmission loss for each GL and used in the theoretical acoustic received levels traced in panel (a). For (b) and (c), coefficient *a* indicates the fitted linear dependence on GL, with the corresponding R^2.

at GL ≈ 9.1 m for our configuration. This could contribute to the weaker variation in NL among the shortest GLs.

The SNR results further demonstrate that the effect of GL depends on spatial geometry. The localized enhancement observed for GL20 is consistent with the greater directional sensitivity expected for longer GLs [18]. Overall, GLs from 8 to 12 m provided comparatively high SNR over a broader portion of the cable at 100 Hz. This range agrees reasonably well with theoretical predictions: the SNR-peak relationship [17] gives a GL of ~ 8.5 m under our conditions, whereas the signal-preservation criterion [19] gives ~ 6.9 m. These values correspond to a simple axial case ($\theta = 0$). The optimal gauge length depends on the apparent wavelength of the wavefield along the cable, i.e., the wavelength projected onto the fiber axis, which varies with propagation geometry [19] and is written as $\lambda_{\mathrm{app}} = c/(|\cos\theta| f)$. Using the revised approximation GL $\approx 0.47\lambda_{\mathrm{app}}$, the predicted optimum at 100 Hz and $c = 1,460$ m/s increases from approximately 7.3 m at $\theta = 20°$ to 20.1 m at $\theta = 70°$. The comparatively strong performance of GL8, GL10 and GL12 is therefore consistent with the range expected over the grazing angles encountered in the analyzed 3 km cable section.

This angular dependence also implies that, for marine mammal monitoring, no single GL is expected to maximize sensitivity for all source positions. Although a spatially variable optimal GL presents a challenge for whale monitoring, it may also provide an opportunity in environments such as the St. Lawrence Estuary, where species distribution and habitat use are relatively well characterized [32]. Combined with species-specific acoustic characteristics and known cable geometry, ecological information could help characterize *in situ* detection probabilities.

V. Conclusion

This experiment shows that gauge length influences multiple components of the DAS response, including pressure-to-strain conversion, noise level, and SNR. At 100 Hz, a GL of 10 m provided the most consistently high SNR across the analyzed cable section. The observed GL dependence varied with source-to-cable geometry and was not fully captured by the theoretical response. These results provide an *in situ* basis for GL selection at 100 Hz and highlight the need to account for source-to-cable geometry when characterizing DAS performance for marine monitoring.

Acknowledgment

We would like to thank TELUS for providing access to their cable infrastructure and facilities, as well as for the support provided by their staff throughout this project. We are grateful to DRDC for providing technical support during the playbacks, and to local students for helping out with marine mammal observation duties. This work was conducted as part of a collaboration between ISMER-UQAR, the Cornell K. Lisa Yang Center for Conservation Bioacoustics, Parks Canada, Merinov, and Agence Mamu Innu Kaikusseth (AMIK).

References

[1] A. H. Hartog, *An introduction to distributed optical fibre sensors*. CRC press, 2017.

[2] D. Rivet, B. de Cacqueray, A. Sladen, A. Roques, and G. Calbris, “Preliminary assessment of ship detection and trajectory evaluation using distributed acoustic sensing on an optical fiber telecom cable,” *The Journal of the Acoustical Society of America*, vol. 149, no. 4, pp. 2615–2627, 2021.

[3] W. Huang, K. Wang, P. Liu, W. Xing, and W. Gan, “Experimental Study on Optoelectronic Submarine Cable Used for Ship Radiation Noise Detection,” *IEEE Access*, vol. 12, pp. 192 731–192 742, 2024.

[4] S. Horne, A. L. Stork, and F. Stanek, “Observations of fin whales and vessels offshore oregon using fibre optic distributed acoustic sensing,” *Frontiers in Marine Science*, vol. 12, 2025-07-03.

[5] M. Landrø, L. Bouffaut, H. J. Kriesell, J. R. Potter, R. A. Rørstadbotnen, K. Taweesintananon, S. E. Johansen, J. K. Brenne, A. Haukanes, O. Schjelderup *et al.*, “Sensing whales, storms, ships and earthquakes using an arctic fibre optic cable,” *Scientific Reports*, vol. 12, no. 1, p. 19226, 2022.

[6] L. Bouffaut, K. Taweesintananon, H. J. Kriesell, R. A. Rørstadbotnen, J. R. Potter, M. Landrø, S. E. Johansen, J. K. Brenne, A. Haukanes, O. Schjelderup *et al.*, “Eavesdropping at the speed of light: Distributed acoustic sensing of baleen whales in the arctic,” *Frontiers in Marine Science*, p. 994, 2022.

[7] W. S. Wilcock, S. Abadi, and B. P. Lipovsky, “Distributed acoustic sensing recordings of low-frequency whale calls and ship noise offshore central oregon,” *JASA Express Letters*, vol. 3, no. 2, p. 026002, 2023.

[8] I. C. Avila, K. Kaschner, and C. F. Dormann, “Current global risks to marine mammals: taking stock of the threats,” *Biological Conservation*, vol. 221, pp. 44–58, 2018.

[9] I. Schwartz-Belkin and M. E. Portman, “A review of geospatial technologies for improving marine spatial planning: Challenges and opportunities,” *Ocean & Coastal Management*, vol. 231, p. 106280, 2023.

[10] R. Gibb, E. Browning, P. Glover-Kapfer, and K. E. Jones, “Emerging opportunities and challenges for passive acoustics in ecological assessment and monitoring,” *Methods in Ecology and Evolution*, vol. 10, no. 2, pp. 169–185, 2019.

[11] J. Delarue, M. Laurinolli, and B. Martin, “Bowhead whale (Balaena mysticetus) songs in the Chukchi Sea between October 2007 and May 2008,” *The Journal of the Acoustical Society of America*, vol. 126, no. 6, pp. 3319–3328, 2009.

[12] R. S. Payne and S. McVay, “Songs of humpback whales,” *Science*, vol. 173, no. 3997, pp. 585–597, 1971.

[13] M. F. Baumgartner and D. M. Fratantoni, “Diel periodicity in both sei whale vocalization rates and the vertical migration of their copepod prey observed from ocean gliders,” *Limnology and Oceanography*, vol. 53, pp. 2197–2209, 2008.

[14] S. E. Parks and P. L. Tyack, “Sound production by north atlantic right whales (eubalaena glacialis) in surface active groups,” *The Journal of the Acoustical Society of America*, vol. 117, no. 5, pp. 3297–3306, 2005.

[15] E. Fleishman, D. Cholewiak, D. Gillespie, T. Helble, H. Klinck, E.-M. Nosal, and M. A. Roch, “Ecological inferences about marine mammals from passive acoustic data,” *Biological Reviews*, vol. 98, no. 5, pp. 1633–1647, 2023.

[16] L. Bouffaut, “Distributed Acoustic Sensing for Marine Mammal Monitoring,” 2026, preprint.

[17] T. Dean, T. Cuny, and A. H. Hartog, “The effect of gauge length on axially incident p-waves measured using fibre optic distributed vibration sensing,” *Geophysical Prospecting*, vol. 65, no. 1, pp. 184–193, 2017.

[18] A. Xenaki, P. Gerstoft, E. Williams, and S. Abadi, “Overview of distributed acoustic sensing: Theory and ocean applications,” *The Journal of the Acoustical Society of America*, vol. 158, no. 1, pp. 801–825, 2025.

[19] T. Cuny, P. Bettinelli, and J. Le Calvez, “Variable gauge length: Processing theory and applications to distributed acoustic sensing,” *Geophysical Prospecting*, vol. 73, no. 1, pp. 160–187, 2025.

[20] L. Bouffaut, M.-E. Clark, B. Jones, G. Hardwick, E. Snyder, P. Cauchy, and H. Klinck, “Playback protocol for in-situ characterization of distributed acoustic sensing in ocean acoustics,” https://github.com/DAS4Whales/playback-protocol, 2026, gitHub repository.

[21] L. Bouffaut, Q. Goestchel, R. A. Rørstadbotnen, A. Sladen, A. Hartog, and H. Klinck, “Estimating sound pressure levels from distributed acoustic sensing data using 20 Hz fin whale calls,” *JASA Express Letters*, vol. 5, no. 4, p. 040802, 2025.

[22] K. Taweesintananon, M. Landrø, J. K. Brenne, and A. Haukanes, “Distributed acoustic sensing for near-surface imaging using submarine telecommunication cable: A case study in the Trondheimsfjord, Norway,” *Geophysics*, vol. 86, no. 5, pp. B303–B320, 2021.

[23] L. Bouffaut, “Das4whales: A python package to analyze distributed acoustic sensing (das) data for marine bioacoustics (v0.1.0),” 2023. [Online]. Available: https://doi.org/10.5281/zenodo.7760187

[24] M. D. Collins, “RAM, RAMS, RAMGeo, RAMSurf,” https://oalib-acoustics.org/models-and-software/parabolic-equation/, 1999, accessed July 20, 2026.

[25] ——, “A split-step Padé solution for the parabolic equation method,” *The Journal of the Acoustical Society of America*, vol. 93, no. 4, pp. 1736–1742, 1993.

[26] F. B. Jensen, W. A. Kuperman, M. B. Porter, and H. Schmidt, *Computational Ocean Acoustics*, 2nd ed., ser. Modern Acoustics and Signal Processing. New York: Springer, 2011.

[27] N. Pinet, V. Brake, C. Campbell, and M. Duchesne, “Seafloor and shallow subsurface of the st. lawrence river estuary,” *Geoscience Canada*, vol. 38, no. 1, pp. 31–40, 2011.

[28] M. J. Duchesne, N. Pinet, A. Bolduc, K. Bédard, and D. Lavoie, “Seismic stratigraphy of the lower st. lawrence river estuary (quebec): Quaternary deposits and seismic signature of the underlying geological domains,” Geological Survey of Canada, Current Research 2007-D2, 2007.

[29] P. J. Barrett and P. C. Froggatt, “Densities, porosities, and seismic velocities of some rocks from victoria land, antarctica,” *New Zealand Journal of Geology and Geophysics*, vol. 21, no. 2, pp. 175–187, 1978.

[30] S. Abadi, “Estimating ship source levels using distributed acoustic sensing data and validation with hydrophone measurements,” *JASA Express Letters*, vol. 6, no. 8, p. 087501, 2026.

[31] T. Dean, A. Hartog, T. Cuny, and F. Englich, “The Effects of Pulse Width on Fibre-optic Distributed Vibration Sensing Data,” in *78th EAGE Conference and Exhibition 2016*. European Association of Geoscientists & Engineers, 2016, pp. 1–5.

[32] A. Mosnier, J.-F. Gosselin, and V. Lesage, “Seasonal distribution and concentration of four baleen whale species in the St. Lawrence Estuary based on 22 years of DFO observation data,” pp. iv+119, 2022.